

Water confined between graphene layers: the case for a square ice

Niels R. Walet*

*Theoretical Physics Division, School of Physics and Astronomy, University of Manchester, M13
9PL, UK*

E-mail: Niels.Walet@manchester.ac.uk

Abstract

Water confined between two graphene layers with a small separation forms a two-dimensional ice structure, with an apparent square symmetry [Algara-Siller *et al.*, Nature (London) **519**, 443 (2015)], which is poorly understood. A density functional approach is applied to the water, but not to the water-graphene interactions, since the two crystals are incommensurate. We thus need use a potential model for the interaction between water and graphene. We analyze the models for confinement of water by graphene, and find that even though the general features are well established, the detail is not so well understood. Using a representative range of potential models, we perform density-functional calculations and show that many ice-like configurations exist. In some cases these are unstable with respect to decay into a bi-layer structure, but we expect tunneling between such structures to be slow. It is shown that there is one good candidate for a square crystal, which is a peculiar anti-ferroelectric arrangement of water molecules.

Considering how important water is in our daily life, it should come as no surprise that understanding its behavior in all kinds of situations is of great interest, even in rather special ones.

*To whom correspondence should be addressed

One recent example is water confined at the nanoscale, which has been studied extensively theoretically,^{1–15} and received a considerable boost following the discovery of a square crystal when water is confined between two layers of graphene.¹⁶

The experiments seem to show a perfect square crystal structure, and indications are that this is not a bilayer structure where one layer is offset relative to the other (so-called AB stacking). Bilayer structures are also seen in the experiment, and claims are made that this is consistent with AA stacking.¹⁵ The oxygen-oxygen distance is quoted as 2.8 Å. In the paper by Algara-Siller *et al.*¹⁶ a classical molecular dynamics calculation is also reported, that shows some aspects of agreement with the experiment, but seems to indicate a rhombic crystal. Such results should be taken with a grain of salt, since potential models are notoriously unreliable for water.¹⁷ This is one of the reasons why so many potential models exist.^{18–24} One of the problems of all these models is a poor description of the higher electric multipole moments (beyond dipole), which are expected to be important in the behaviour of water.²⁵ Indeed, the results of the MD simulations¹⁶ show a rhombic ice, where thermal motion needs to be invoked to show a structure that is square on average, which feels slightly artificial, but may be possible.

To avoid the uncertainty of potential models a number of investigations have used density functional theory to describe the interaction of the water molecules, employing simple confining potentials to account for the effect of graphene. Using such an approach one can only study the zero-temperature ground state, which may be a draw-back, unless this structure is energetically well separated from other states. We are aware of one study²⁶ that looks at a water layer in front of a single layer of graphene using DFT at finite temperature, but none that look at the problem at hand. On the other hand there are a number of fully microscopic calculations of water in front of finite but large flat carbon molecules have been performed.^{27–32} These have been extrapolated to graphene, and probably give a decent estimate of the binding and orientational dependence of the binding of water to graphene. The long-range behavior of all such models is r^{-6} , showing the fact that the large but finite carbon molecules are all insulators—unlike real graphene, which is a semi-metal. Nevertheless, we shall use these results to build improved models. There are many

ways to model the interaction of water with graphene. We shall use a simple surface-integrated Lennard-Jones potential (3-9 potential) which has the correct asymptotics,³³ but a rather arbitrary choice of core repulsion (see below).

One of the other problems that all investigations face is the choice of thermodynamic potential to be optimized when describing confined water—this is a thorny question, and most papers adopt a form of 2D enthalpy linked to the inter-layer separation distance and the in-plane stress (rather than the 3D pressure). There is no obvious reason to look at constant stress; the real situation is much more complicated than in an ideal 2D baryostat, since the vertical stresses must have an influence on the separation of the graphene layers.

We approach the problem in a slightly different way: we report a set of DFT calculation of a model system at a density corresponding exactly to the experimental one (one H₂O molecule per (2.8 Å)²). The picture that underlies this idea is that the graphene response to stresses is rather complex, with layers separating rather suddenly if a pressure/stress threshold is reached. As long as stresses are relatively small, that is probably a reasonable approach to take; when the vertical stress increases, we expect the graphene layers to separate further and accommodate multiple layers. This is actually an example of a well-established mechanism, which is used in the production of intercalated graphite compounds.³⁴

We will first, in the next section, investigate the nature of the confinement water by graphene and the interaction of water with graphene, including how the interaction depends on the orientation of the water molecule. Then we analyze in some detail, in the next section, DFT calculations and the dependence on the confining potential. In the final section we give look at conclusions and potential further work.

Confinement of water by graphene

Water-graphene interaction potential

We first investigate the nature of the confining potential. The interaction of water with graphene has been studied microscopically, using coupled cluster theory,^{27,32} many-body perturbation theory^{28,30} and a DFT/perturbation theory hybrid.^{29,31} These results set a benchmark: a maximal attraction of in the order of 100 – 130 meV per molecule at a distance of about 3.2Å. The detailed data on distance dependence in figure 2 of Voloshina *et al.*³² seems to show an attraction that falls as r^{-6} , which appears inconsistent with the semi-metallic nature of graphene, and probably reflects a limitation of the extrapolation to graphene of a long-range interaction of water with a finite carbon molecule, which unlike graphene is insulating. It also shows, in the region where the calculations must be more reliable, since it is dominated by electronic correlations, a soft repulsive core that is poorly fitted by an inverse power law. Most importantly for the work reported here, the harmonic part of the potential about equilibrium is rather small, and much less than estimated from a van-der-Waals potential (3 – 9) or 6 – 12). The attraction between water and graphene depends on the water orientation and its position relative to the graphene layer, but this is not the case for the equilibrium distance of the molecule relevant to graphene. This can be compared to the finite-temperature DFT (and thus infinite through the use of periodic boundary conditions) calculations in,²⁶ which suggest that a randomly oriented water slab sitting in front of a single graphene layer feels a potential (lowest curve in their figure 4) that can be fitted by an $1/r^3$ long range attractive force, again with a weak repulsive kernel that does not seem to follow a simple power law—definitely not the strong repulsion used in most works on the subject.¹

For our calculation, based on the experiment where the ice crystals are incommensurate with graphene, we can not describe the graphene and water simultaneously in full microscopic detail,

¹Part of this discrepancy may be due to their definition of separation as the distance of the nearest hydrogen atom to the graphene layer, which is inconsistent with the more common definition of the distance from the oxygen molecule or almost equivalently the center-of-mass to the graphene layer. The distance quoted is therefore always smaller than the usual definition of distance, since, as the authors state, the Hydrogen bonds prefer to point towards the graphene layer.

and we need a potential model to describe part of it—as usual we do this for the graphene-water interaction. There are a number of models for the interaction between a material such as graphene and water; some (e.g.¹⁴) use the 3 – 9 hydrophobic interaction first proposed by Lee *et al.*;³⁵ Chen *et al.*³⁶ use a Morse potential fit to a rather scattered set of GFMC data, and modern potential models for water in carbon-nanotubes (see, e.g.,^{37–41}) suggests a fit of the interaction between water and carbon atoms as a combination of C-O and C-H 6 – 12 Lennard-Jones potentials.

Actually we only need a full model of the potential for our discussion of graphene bubbles below, whereas in the rest of the paper it will suffice to look at a harmonic expansion. For the analysis below we mainly use the simplest model, an interaction between the graphene and the oxygen in the water molecule only. In the light of the discussion above, we choose a 3 – 9 potential of the form

$$V_{39}(z) = V_0 \left[\frac{1}{2} \left(\frac{\sigma}{z} \right)^9 - \frac{3}{2} \left(\frac{\sigma}{z} \right)^3 \right], \quad (1)$$

where for the water-graphene potential, $V_{39}^{wg}(z)$, we use

$$V_{0,wg} = 120 \text{ meV}, \quad \sigma_{wg} = 3.2 \text{ \AA}. \quad (2)$$

The strength used here is just a suitable average of the microscopic values, which range from –100 to –135 meV/molecule, but do depend on position and orientation relative to the graphene layer. The equilibrium position is a similar average, but is not very sensitive to position or orientation.³²

One simple way to include the directionality of the water-graphene interaction is to fit two 3-9 potentials (??) to the microscopic data, a graphene-O and a graphene-H one. For all the reasons discussed above, this has an unreasonably large harmonic behavior and also lacks the dipole–semi-metal long-range interaction,³³ but with limited data available this is probably the best we can do. We fit the results³² with a form

$$V(z, \theta) = V_{39}^{Og}(z) + V_{39}^{Hg}(z + b \cos(\phi_b/2 + \theta)) + V_{39}^{Hg}(z + b \cos(-\phi_b/2 + \theta)), \quad (3)$$

where θ is the angle of the dipole moment with the normal, assuming that the Hydrogen atoms are always in a plane perpendicular to the graphene layer. We find that the strength parameters are

$$V_{0,Og} = 77.7 \text{ meV}, \sigma_{Og} = 3.14 \text{ \AA}, V_{0,Hg} = 24.3 \text{ meV}, \sigma_{Hg} = 2.73 \text{ \AA}, \quad (4)$$

which reflects the fact that for a single layer the dipole moment points preferentially towards the graphene layer.

Graphene bubbles

Graphene bubbles are rather difficult to model, because there are many different situations we can consider. It seems likely that for thin layers of water confined between graphene, the model of Guinea [F. Guinea, Pressure inside crystalline bubbles confined by graphene, 2016] applies. This models an extended bubble with height much smaller than its width, which is flat in the middle, and has a smooth connection to the underlying substrate of width d . Of course more complex models can be constructed; the best type of mechanical model is probably one based on thin-plate theory (see, e.g.,⁴²), but even that has weaknesses, since adhesion is quite a complex phenomenon, as for instance discussed by Sprigman and collaborators.⁴³ We shall ignore all such complexity, and use the simple model, since here we are more interested in the phase inside the bubble than the exact details of the shape and dynamics of the bubble.

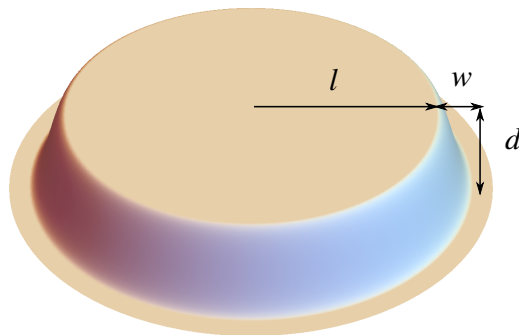


Figure 1: A graphical representation of the confinement model. We assume that the boundary is sharp, $w \ll l$, and that the height d is constant, apart from the boundary region, with $d \ll l$.

Many discussions use “pressure” as the quantity describing the confined phase. This is not correct: it is straightforward to show that the stress in the direction perpendicular to the graphene is very different from that in the two directions parallel to the layers. If we assume a cylindrical bubble, it seems reasonable to assume the in-plane stress is diagonal and equal in both directions, and this may be what other work calls the “pressure”. As we shall see the in-plane stresses range from 0.1 GPa upwards, whereas the vertical stress, to be defined below, at the experimental density should be small. Stresses are calculated as the variation of energy with the dimensions of the simulation box, which lacks some of the detailed information that might be of interest, since the horizontal force for a layered system is most likely to be strongest at the height of the confined layer(s), and almost zero near the graphene layers. Nevertheless, with the data available we can construct a crude model of how graphene confines the water. We first ignore the internal elasticity of graphene, and assume the water to be confined inside a pill-box shaped graphene container of radius l , see figure 1. If we assume that the area of bubble is much larger than the graphene spacing, we can determine the equilibrium distance ignoring the sides, by minimizing the potential energy per unit area.

We model this by a total of three 3 – 9 potentials; two representing the interaction between two layers of water (assumed at a distance $(d \pm d_1)/2$ of each of the two graphene layers) and each of the two graphene layers, and one for the attraction between the two graphene layers at distance d ,

$$V(d, d_1) = V_{39}^{wg}((d + d_1)/2) + V_{39}^{wg}((d - d_1)/2) + V_{39}^{gg}(d). \quad (5)$$

Here the water-graphene potential V^{wg} was already introduced above and we denote by $V^{gg}(d)$ the potential energy per unit area for two graphene layers in vacuum at separation d . If we take the GFMC calculations⁴⁴ as a benchmark, we find that a reasonable value for $V_{0,gg} = -V_{39}^{gg}(d_0)$ is about $8 \text{ meV}/\text{\AA}^2$, where the equilibrium distance $d_0 = \sigma_{gg} = 3.41 \text{ \AA}$. For water, we use the parameters defined above, $V_{0,wg} = 120/2.8^2 = 15.3 \text{ meV}/\text{\AA}^2$. If we ignore the edges of the bubble, i.e., $l \gg d, w$, we can minimize the energy per unit area Eq. (??) to find that the optimal configuration

is a single layer of water in the middle of two graphene layers separated by $d = 6.36 \text{ \AA}$, which is very close to $2\sigma_{wg}$, since the water-graphene potentials are stronger than the graphene-graphene one. This also means that this result is essentially independent of the potential model, since it is mainly sensitive to the equilibrium distance and binding energy.

For generality, we shall look at the energy associated with the classical potentials of a bilayer of water, a distance $(d \pm d_1)/2$ from the graphene layers,

$$E = \pi l^2 \Delta V^{gg}(d) + \pi l_0^2 (V^{wg}((d + d_1)/2) + V^{wg}((d - d_1)/2)). \quad (6)$$

Here $\Delta V^{gg}(d) = V_{39}^{gg}(d) - V_{39}^{gg}(d_0)$, and l_0 is the length parameter where we have evaluated the water-graphene interaction parameters; since the number of water molecules is fixed, in reality the energy depends on the numbers of water molecules, not on the size of the bubble. The horizontal force exerted by the graphene on the water due to a change in the radius l is thus $F = 2\pi l \Delta V^{gg}$. If the in-plane stress tensor of the water is diagonal with equal magnitude, $S_x = S_y = S$, we see that the average force on the rim of the bubble is $2\pi l \Delta d S$, which must balance the force exerted by the bubble due to the interactions between the water molecules. Comparing the two expressions for the force, we find the relation

$$S = \Delta V^{gg}(d)/\Delta d. \quad (7)$$

This simply states that the stress of confinement balances the horizontal stress exerted by the confined water. If we use $d = 6.4 \text{ \AA}$, we find $\Delta V^{gg} \approx 6 \text{ meV/\AA}^2$ which is somewhat dependent on the potential model. This then gives a value for $S = S_{x,y}$ of the order of $S = 0.5 \text{ GPa}$, which is rather similar to the numbers found experimentally by Vasu *et al.*,⁴⁵ which are maybe a factor of 2 higher. Our estimate could potentially vary by factors of 2 up or down even if we were to know ΔV^{gg} more accurately: As shown by Guinea the elastic energy of graphene tends to increase the force exerted on the water, whereas the expected inhomogeneity of the force exerted by the layer of water tends to induce a stronger curvature of the side of the graphene, thus supporting a lower stress. This analysis is only valid in the absence of vertical stress. It is quite close to the values of

"pressure" reported by Vasu *et al.*⁴⁵

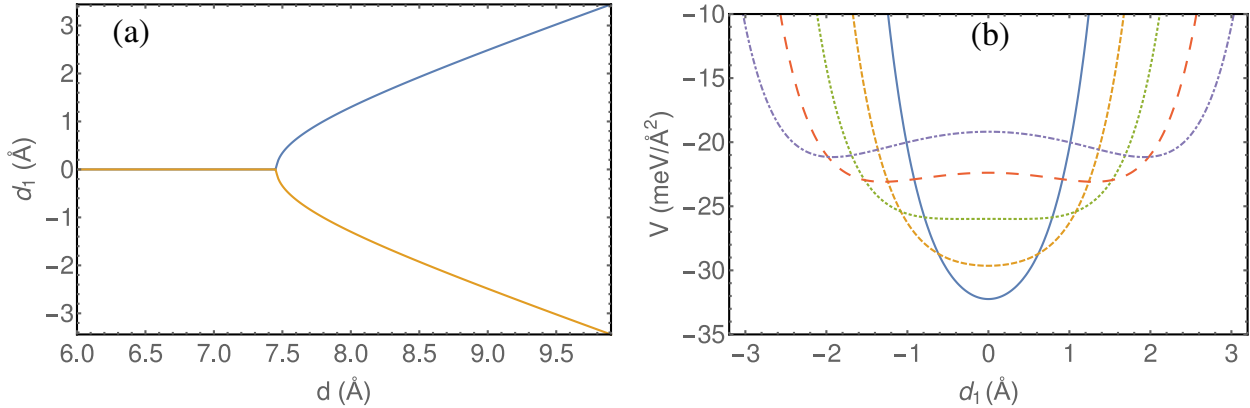


Figure 2: Analysis of the potential energy per unit area V , Eq. (??) as a function of d and d_1 . (a) The optimal choice of the water-water distance d_1 as a function of the graphene-graphene distance d . At $d = 7.45$ Å bilayer forms. (b): The shape of the potential V as a function of d_1 for $d = 6.5$ Å (solid blue line), $d = 7$ Å (yellow dashed line), $d = 7.5$ Å (red dotted line), $d = 8$ Å (green long-dashed line) and $d = 8.5$ Å (purple dot-dashed line).

If we artificially increase the separation between the layers, i.e., look at the optimal values of d_1 for fixed d , see figure 2, we find that the potential becomes shallow quite quickly. As we force the graphene layers further apart, there is a sudden transition from a single water layer to a bilayer—for our simple model this bifurcation occurs at $d = 7.45$ Å.

Since the water itself also exerts a vertical stress, the picture changes: as we increase the density both horizontal and vertical stress will increase, leading either to an increase in radius of the bubble, or an increase in height with the concomitant formation of a bilayer, which may induce some of the snap transitions discussed in the literature.⁴³ The vertical force exerted by the graphene can be calculated as $F = \pi l^2 \partial_d V^{gg}$. If d is almost the equilibrium distance as shown above, this is almost zero, and thus the vertical stress is almost zero as well. When the stress of the water increases, we see that we must move away from this equilibrium. At the same time the reaction force to the confining potential also contributes, and we need to balance stress from the water, the attraction exerted by the water due to confinement, and the graphene-graphene interaction. If we use the potential model sketched above, we find this is mainly sensitive to the harmonic part of the water-graphene potential. If we use the 3 – 9 potentials as above (which leads to too large a curvature of the potential), we find that the graphene layer moves roughly 0.3 Å/GPa; this is clearly strongly

dependent on the potential model, but suggests that realistic numbers are less than 10 times that value, which is still a small effect, if we realize that stresses are typically less than 1 GPa.

Orientalional order

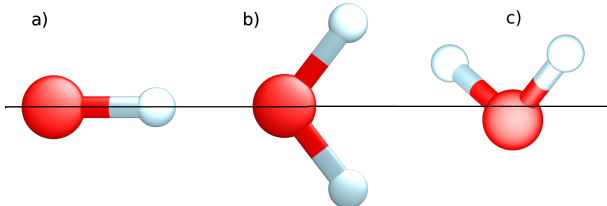


Figure 3: The three positions of a water molecule considered for interactions, when confined between two metallic layers at distance 5\AA parallel to the black line, and perpendicular to the paper. The black line gives the mid-point between the layers, and the positions of the atoms are the ones obtained after optimization (most important for case c).

Table 1: The energy gain of a water molecule placed between two metallic layers, as compared to the same molecule in vacuum, see figure 3 for details.

case	energy gain
a	-12.5 meV
b	-19.2 meV
c	-57.5 meV

We now look at the orientation dependence of the energy of a water molecule between 2 graphene layers, which is an important secondary aspect of the problem. We shall use input from microscopic calculations using water in position c) in figure 3 relative to a *single* layer of graphene. For the case of a bilayer, it is relatively straightforward to show³³ that the interaction of a point dipole between two graphene layers has a preferential orientation. In the RPA approximation for graphene, if the dipole makes an angle θ with respect to the vertical to the layers, we can find an analytical expression.³³ Using this with $d = 5\text{\AA}$, and $p = 1.85\text{ D}$ for water, we then find $V = -(31 + 51 \cos^2 \theta)$ meV for a metal ($\epsilon_r = \infty$), which gets reduced to $V = -(21 + 29 \cos^2 \theta)$ meV for two free-standing graphene layers with the estimate $\epsilon_r = 5$. This is entirely consistent with the variation seen in the microscopic calculations cited above (but there

one normally only considers a single layer with the two realizations of case c, with the dipole moment pointing to or away from graphene), suggesting this is a relevant effect.

We have also calculated these numbers for a slightly more realistic description of water, using a slightly augmented version of the approach as used below for ice: we use the EMS method⁴⁶ within a DFT calculation using quantum espresso,⁴⁷ which makes it possible to add electrostatic boundary conditions and remove the usual 3D periodicity on the direct interactions, to study a single water molecule between two perfectly structureless metallic layers ($\epsilon_r = \infty$)², separated by 5Å to enhance the effect of the boundaries. We compare the energy difference between for same molecule between two metallic layers ($\epsilon_r = \infty$), and two layers of vacuum ($\epsilon_r = 0$) for the three configurations shown in figure 3], with a structural optimization that keeps the orientation of the water molecule. The interesting aspect is the difference between cases a) and b), which is not analyzed in detail in the microscopic work. As we can see from table 1 we find a substantial effect of about 45 meV, in reasonable agreement with the more accurate calculations above. All of this indicates the effect of the polar interactions; it probably misses some of the additional hydrogenic interactions with graphene seen in the calculations.

Results

We now perform a first principle study of water confined between graphene using density-functional theory (DFT). We immediately need to face two problems: which of the many functionals to choose, and how to model the confinement. Water is a notoriously difficult system to describe using DFT, as reviewed by Gillan *et al.*⁴⁸ All good simulations require van-der-Waals exchange functionals, and for layered systems and water a combination of van-der-Waals exchange with optimized exchange potentials appears to be important. For that reason, and the fact that our simulations are performed with quantum espresso,⁴⁷ we shall compare results using two functionals,

²Even though the case of finite ϵ_r is discussed by Ottani *et al.*,⁴⁶ this case is not actually implemented in the quantum espresso code, since it requires an additional model-dependent solver step, where a charge distribution must be inferred [M. Otani, private communication]

Table 2: Energy per molecule, compared to the lowest energy solution for those configurations within 50 meV of the ground state. The accuracy of the energies is about 1 meV, for the stresses about 0.02 GPa. We compare three values of the confinement width (modeled by using a 3-9 potential with appropriate strength).

configuration	$\alpha = 350\text{meV/\AA}^2$				$\alpha = 200\text{meV/\AA}^2$				$\alpha = 50\text{meV/\AA}^2$			
	ΔE meV	ΔE_{conf} meV	$S_{x,y}$ GPa	S_z GPa	ΔE meV	ΔE_{conf} meV	$S_{x,y}$ GPa	S_z GPa	ΔE meV	ΔE_{conf} meV	$S_{x,y}$ GPa	S_z GPa
corrugated I	44.6	7.2	0.6	0.03	16.4	43.9	0.16	0.13	-69.3	29.0	-0.12	0.1
corrugated II	30.0	4.3	0.5	0.04	-18.8	36.4	-0.04	0.13	32.2	52.9	0.36	0.09
corrugated III	15.0	30.2	0.29	0.1	9.9	36.4	0.14	0.13	-70.4	26.1	-0.11	0.12
corrugated IV	20.6	37.1	0.28	0.1	11.7	42.1	0.13	0.12	-72.5	28.4	-0.13	0.1
corrugated V	0	18.2	0.28	0.06	1.7	23.7	0.17	0.1	-70.6	20.2	-0.07	0.11
corrugated VI	0.1	15.6	0.31	0.03	0	30.9	0.15	0.08	-75.8	25.3	-0.12	0.08
in-plane I	123.	0	0.82	0.01	137.	0	0.82	0.01	104	0	0.82	0.02
in-plane II	81.0	0	0.59	0.	95.	0	0.6	0.	62.2	0	0.6	0.01
in-plane III	21.6	0.2	0.5	0.01	34.5	0.4	0.5	0.02	-54.7	28.0	-0.03	0.12
in-plane IV	81.0	0	0.54	0.02	14.8	0.9	0.4	0.03	62.2	0	0.55	0.01
in-plane V	5.2	0	0.54	-0.01	19.0	0	0.53	-0.01	-75.8	25.4	-0.12	0.09
out of plane square	34.5	15.6	0.41	0.07	41.7	9.4	0.44	0.06	0	3.4	0.39	0.02

vdW-DF⁴⁹⁻⁵² and compare to numbers from vdW-DF-ob86.⁵³ In each case confinement is implemented as an external 3-9 potential acting on the O nuclei. Its effect is actually surprisingly small on the structures—but of course that may be different for their stability. The most important difference between our work and previous work that looked at the faces of confined water is that we work at constant density, and minimize the energy with respect to the shape of the unit cell, rather than an artificially designed 2D enthalpy. As other calculations, we work at zero temperature.

We have used a structure search which, rather than completely random, is based on the configurations found in the literature³. These correspond to states with all the oxygen atoms in a single plane, or ones where the oxygen atoms form a slightly corrugate plane. Additional detail can be found in the supplementary material. Considering the potential orientational energy gains, one must consider all configurations where the energy per molecule is less than $\simeq 50$ meV, and then weigh which ones may be favored. We use results from the literature^{14,36} to select potentially appropriate candidates,⁴ and then minimize the energy of such states, first with respect to position in the unit cell, and then with respect to the shape of the unit cell, keeping the density fixed. Stable minimum energy solutions for any given density then have isotropic 2D stress. Labeling of the

³We have also tried some random searches, but have not found any states other than the out-of-plane square.

⁴We have also tried some random searches, but have not found any states other than the out-of-plane square.

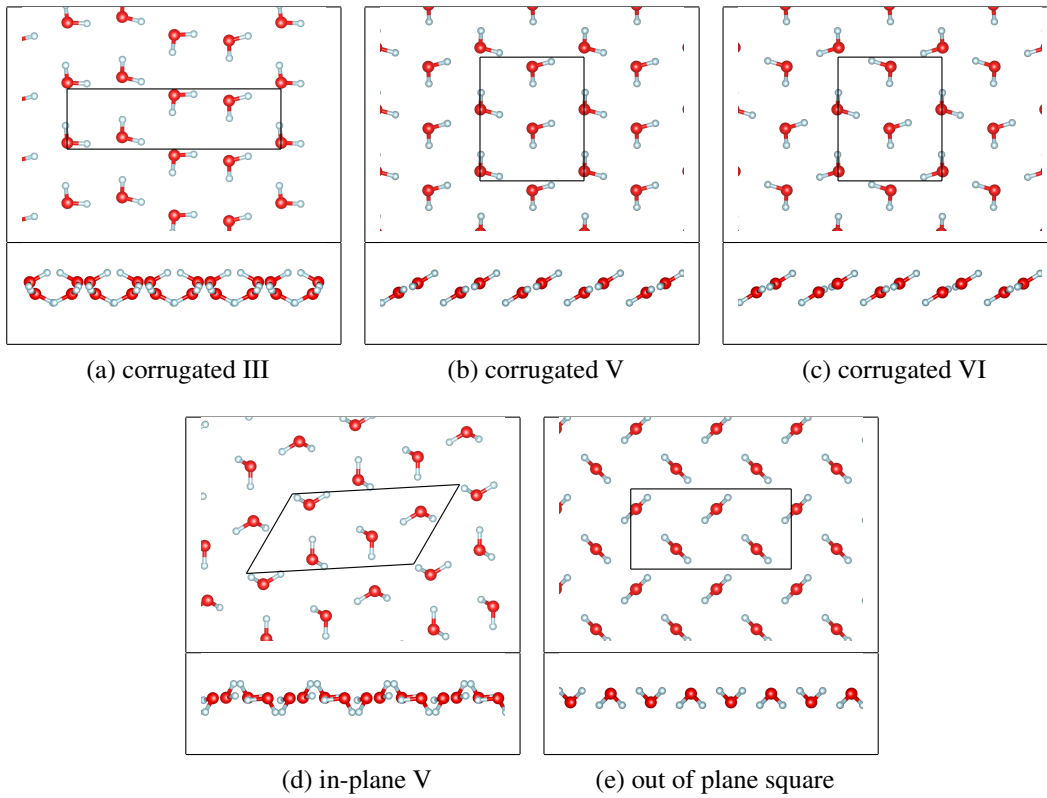


Figure 4: A summary of the most relevant configurations. They are shown here for the strongest confinement, $\alpha = 350\text{meV}/\text{\AA}^2$; the area delimited by the black lines shows the optimized 2D unit cell.

configurations is with the initial configurations—see the references for details. Numerical details of the results can be found in table 2.

We show some of the key configurations in figure 4, where we selected the strong confining potential; the main visual difference for weaker confinement is a further separation of the “square” configurations in a bilayer like structure. The lowest energy states (for this confinement) both have a rhombic unit cell—in this case it looks like there is a perfect equilateral triangular crystal, but with rather different dipole orientations. The real surprise is the perfectly square crystal state, which seem relatively insensitive to the detail of the confining potential.

The water molecules experience very little confinement in the lowest energy solutions, and the vertical stresses (indicative of how hard the water pushes on the graphene, separating the layers) are small, as can be seen from Table 2. In that table, we label the states with the initial seeding configuration—which in some cases is close to the final result. This is the case where we want to concentrate most clearly on the effect of the confining potential. All of these are single layers, with some corrugation, but even for a weak confining potential we find that all oxygens are located very close to $d/2$. We can thus investigate the effect of moderate changes in the confining potential by just look at the harmonic potential dependence around the midpoint, $E = \alpha \delta r^2$. We take the value obtained from the 3 – 9 potential ($\alpha = 350\text{meV}/\text{\AA}^2$), which is probably unrealistically steep about the minimum due to the very strong repulsive core, as an upper estimate. We will use $\alpha = 50, 200$ and $350\text{meV}/\text{\AA}^2$ to investigate this dependence.

As we can see in table 2, the ordering of the states and the stresses are rather sensitive to the choice of this parameter. For the strongest confinement, we find that those configurations relaxed from a slightly out of plane rhombic unit cell give by far the lowest energies, but in some cases with substantial vertical stresses. As we decrease the confinement, the vertical stress gets larger, corresponding to a tendency towards forming bilayers, and for the lowest harmonic strength we find a tendency to form bilayers—which prefer a slightly higher density inside each layer, thus leading to negative stress. For the flatter honeycomb based states the trend is that we need a slightly larger horizontal stress to confine the water, maybe slightly closer to what we expect the stress to be,

vertical stresses are negligible. As we decrease the confinement, some of these states also start forming bilayers. As we decrease the confinement, the only really square configuration we have found, the anti-ferroelectric states with the dipoles are perpendicular to the graphene, becomes the lowest energy stable state, thus giving at least a natural candidate for a real square crystal.

Finally, we look at the orientation dependent potential Eq. (??). For this case find that the solutions that tend to form a bilayer now have substantial vertical stresses, and are thus probably unstable against an increase in separation of the graphene layers, see table 3. The anti-ferroelectric state gains considerable energy relative to the in-plane solutions, and occurs about 16 meV above the lowest state. This is very suggestive that this definitely needs to be considered as the prime candidate for the ground state, since minor modification to the confining potential can bring its energy down considerably.

Table 3: Energy per molecule, compared to the lowest energy solution for those configurations near the ground state. The accuracy of the energies is about 1 meV, for the stresses about 0.02 GPa. We compare a tight directionless confinement with a directional potential of the same depth and similar range (modeled by a combination of 3-9 potentials with appropriate strengths).

configuration	$\alpha = 350\text{meV}/\text{\AA}^2$				directional			
	ΔE meV	ΔE_{conf} meV	$S_{x,y}$ GPa	S_z GPa	ΔE meV	ΔE_{conf} meV	$S_{x,y}$ GPa	S_z GPa
corrugated I	44.6	7.18	0.6	0.03	18.2	37.0	0.22	0.16
corrugated II	30.0	4.29	0.5	0.04	10.7	30.6	0.20	0.16
corrugated III	15.0	30.2	0.29	0.10	10.7	30.9	0.20	0.16
corrugated IV	20.6	37.1	0.28	0.10	11.3	34.0	0.17	0.14
corrugated V	0	18.2	0.28	0.06	1.64	19.3	0.22	0.13
corrugated VI	0.1	15.6	0.31	0.03	0	26.4	0.2	0.11
in-plane I	123.	0	0.82	0.01	104.	4.16	0.7	0.07
in-plane II	80.9	0	0.59	0.	96.9	4.24	0.61	0.08
in-plane III	21.6	0.233	0.5	0.01	29.7	7.33	0.44	0.06
in-plane IV	81.0	0	0.54	0.02	96.8	4.28	0.55	0.06
in-plane V	5.16	0	0.54	-0.01	17.2	0	0.54	0.02
out of plane square	34.5	15.6	0.41	0.07	33.3	3.74	0.42	0.04

Finally, we still need to consider whether the use of a different van-der-Waals exchange functional might change the results. We have repeated the calculation for the modified DFT function

vdW-DF-ob86, and find that energy shifts by a few meV. Such changes are small compared to the uncertainties in the nature of the confinement, and can thus be safely ignored for now.

Conclusions

We have analyzed some of the effect of confinement on the phases of 2D water. We find that there is a great sensitivity to the nature of the confining potential, but we also see a perfectly good candidate for the observed square crystal. Clearly it is of crucial importance to understand the nature of the confinement experienced of water. It is important in water flow experiments,⁵⁴ and when using graphene anvils.⁴⁵ The next stage of this work will be to get a better understanding of the water graphene interactions from a combination of macroscopic and microscopic methods.

methods

Computational Technology All DFT calculation were performed using the Quantum Espresso code,⁴⁷ version 5.1.2, with modifications to account for the confining potentials. The geometry optimizations were all performed using the vdW-DF exchange functional,⁴⁹⁻⁵² with Perdew-Burke-Ernzerhof (PBE) pseudo potentials. The kinetic energy cutoff was chosen to be 450 eV.

Acknowledgement

The author would like to thank Paco Guinea and Mike Moore for useful discussions regarding the work reported in this paper, and Paco Guinea for sharing his notes on bubble formation. The author would also like to acknowledge the assistance given by IT Services and the use of the Computational Shared Facility at The University of Manchester, where most of the calculations were performed.

Supporting Information Available

A full list of all configurations is given in the supplementary materials, where we also discuss the starting values used. This material is available free of charge via the Internet at <http://pubs.acs.org/>.

References

1. Fraerman, A. A.; Sapozhnikov, M. V. Metastable and nonuniform states in 2D orthorhombic dipole system. *J. Magn. Magn. Mater.* **1999**, *192*, 191–200.
2. Kolesnikov, A. I.; Zanotti, J.-M.; Loong, C.-K.; Thiyagarajan, P.; Moravsky, A. P.; Loutfy, R. O.; Burnham, C. J. Anomalously Soft Dynamics of Water in a Nanotube: A Revelation of Nanoscale Confinement. *Phys. Rev. Lett.* **2004**, *93*, 035503.
3. Kumar, P.; Starr, F. W.; Buldyrev, S. V.; Stanley, H. E. Effect of water-wall interaction potential on the properties of nanoconfined water. *Phys. Rev. E* **2007**, *75*, 011202.
4. Cicero, G.; Grossman, J. C.; Schwegler, E.; Gygi, F.; Galli, G. Water Confined in Nanotubes and between Graphene Sheets: A First Principle Study. *J. Am. Chem. Soc.* **2008**, *130*, 1871–1878.
5. Møgelhøj, A.; Kelkkanen, A.; Wikfeldt, K. T.; Schiøtz, J.; Mortensen, J. J.; Pettersson, L. G. M.; Lundqvist, B. I.; Jacobsen, K. W.; Nilsson, A.; Nørskov, J. K. Ab initio van der Waals interactions in simulations of water alter structure from mainly tetrahedral to high-density-like. *J. Phys. Chem. B* **2011**, *115*, 14149–14160.
6. Kirov, M. V. New Two-Dimensional Ice Models. *J. Stat. Phys.* **2012**, *149*, 865–877.
7. Kirov, M. V. Residual entropy of ice nanotubes and ice layers. *Physica A* **2013**, *392*, 680–688.
8. Anick, D. J. Static Density Functional Study of Graphene–Hexagonal Bilayer Ice Interaction. *J. Phys. Chem. A* **2014**, *118*, 7498–7506.

9. Ramírez, R.; Singh, J. K.; Müller-Plathe, F.; Böhm, M. C. Ice and water droplets on graphite: A comparison of quantum and classical simulations. *J. Chem. Phys.* **2014**, *141*, 204701.
10. Zhao, W.-H.; Bai, J.; Yuan, L.-F.; Yang, J.; Zeng, X. C. Ferroelectric hexagonal and rhombic monolayer ice phases. *Chem. Sci.* **2014**, *5*, 1757–1764.
11. Akashi, R.; Kawamura, M.; Tsuneyuki, S.; Nomura, Y.; Arita, R. First-principles study of the pressure and crystal-structure dependences of the superconducting transition temperature in compressed sulfur hydrides. *Phys. Rev. B* **2015**, *91*, 224513.
12. Chen, J.; Schusteritsch, G.; Pickard, C. J.; Salzmann, C. G.; Michaelides, A. 2D ice from first principles: structures and phase transitions. *Phys. Rev. Lett.* **2015**, *116*, 025501, arXiv: 1508.03743.
13. Standop, S.; Michely, T.; Busse, C. H₂O on Graphene/Ir(111): A Periodic Array of Frozen Droplets. *J. Phys. Chem. C* **2015**, *119*, 1418–1423.
14. Corsetti, F.; Matthews, P.; Artacho, E. Structural and configurational properties of nanoconfined monolayer ice from first principles. *Sci. Rep.* **2016**, *6*, 18651, arXiv: 1502.03750.
15. Sobrino Fernandez Mario, M.; Neek-Amal, M.; Peeters, F. M. AA-stacked bilayer square ice between graphene layers. *Phys. Rev. B* **2015**, *92*, 245428.
16. Algara-Siller, G.; Lehtinen, O.; Wang, F. C.; Nair, R. R.; Kaiser, U.; Wu, H. A.; Geim, A. K.; Grigorieva, I. V. Square ice in graphene nanocapillaries. *Nature* **2015**, *519*, 443–445.
17. Sokhan, V. P.; Jones, A. P.; Cipcigan, F. S.; Crain, J.; Martyna, G. J. Signature properties of water: Their molecular electronic origins. *Proc. Natl. Acad. Sci. U.S.A.* **2015**, *112*, 6341–6346.
18. Mahoney, M. W.; Jorgensen, W. L. A five-site model for liquid water and the reproduction of the density anomaly by rigid, nonpolarizable potential functions. *J. Chem. Phys.* **2000**, *112*, 8910–8922.

19. Ren, P.; Ponder, J. W. Polarizable Atomic Multipole Water Model for Molecular Mechanics Simulation. *J. Phys. Chem. B* **2003**, *107*, 5933–5947.
20. Horn, H. W.; Swope, W. C.; Pitner, J. W.; Madura, J. D.; Dick, T. J.; Hura, G. L.; Head-Gordon, T. Development of an improved four-site water model for biomolecular simulations: TIP4P-Ew. *J. Chem. Phys.* **2004**, *120*, 9665–9678.
21. Rick, S. W. A reoptimization of the five-site water potential (TIP5P) for use with Ewald sums. *J. Chem. Phys.* **2004**, *120*, 6085–6093.
22. Abascal, J. L. F.; Vega, C. A general purpose model for the condensed phases of water: TIP4P/2005. *J. Chem. Phys.* **2005**, *123*, 234505.
23. Fanourgakis, G. S.; Xantheas, S. S. The Flexible, Polarizable, Thole-Type Interaction Potential for Water (TTM2-F) Revisited. *J. Phys. Chem. A* **2006**, *110*, 4100–4106.
24. Fanourgakis, G. S.; Xantheas, S. S. Development of transferable interaction potentials for water. V. Extension of the flexible, polarizable, Thole-type model potential (TTM3-F, v. 3.0) to describe the vibrational spectra of water clusters and liquid water. *J. Chem. Phys.* **2008**, *128*, 074506.
25. Abascal, J. L. F.; Vega, C. The melting point of hexagonal ice (Ih) is strongly dependent on the quadrupole of the water models. *Phys. Chem. Chem. Phys.* **2007**, *9*, 2775.
26. Partovi-Azar, P.; Kühne, T. D. Van der Waals forces from first principles for periodic systems: Application to graphene-water interactions. *arXiv:1504.04649 [cond-mat, physics:physics, physics:quant-ph]* **2015**, arXiv: 1504.04649.
27. Cabaleiro-Lago, E. M.; Carrazana-García, J. A.; Rodríguez-Otero, J. Study of the interaction between water and hydrogen sulfide with polycyclic aromatic hydrocarbons. *The Journal of Chemical Physics* **2009**, *130*, 234307.

28. Jenness, G. R.; Jordan, K. D. DF-DFT-SAPT Investigation of the Interaction of a Water Molecule to Coronene and Dodecabenzocoronene: Implications for the Water-Graphite Interaction. *J. Phys. Chem. C* **2009**, *113*, 10242–10248.
29. Rubeš, M.; Nachtigall, P.; Vondrášek, J.; Bludský, O. Structure and Stability of the Water-Graphite Complexes. *J. Phys. Chem. C* **2009**, *113*, 8412–8419.
30. Jenness, G. R.; Karalti, O.; Jordan, K. D. Benchmark calculations of water–acene interaction energies: Extrapolation to the water–graphene limit and assessment of dispersion–corrected DFT methods. *Phys. Chem. Chem. Phys.* **2010**, *12*, 6375–6381.
31. Kysilka, J.; Rubeš, M.; Grajciar, L.; Nachtigall, P.; Bludský, O. Accurate Description of Argon and Water Adsorption on Surfaces of Graphene-Based Carbon Allotropes. *J. Phys. Chem. A* **2011**, *115*, 11387–11393.
32. Voloshina, E.; Usvyat, D.; Schütz, M.; Dedkov, Y.; Paulus, B. On the physisorption of water on graphene: a CCSD(T) study. *Phys. Chem. Chem. Phys.* **2011**, *13*, 12041–12047.
33. Guinea, F.; Walet, N. R. Interaction between point charges, dipoles and graphene layers. *arXiv:1605.08429 [cond-mat]* **2016**, arXiv: 1605.08429.
34. Ebert, L. B. Intercalation Compounds of Graphite. *Ann. Rev. Mat. Sci.* **1976**, *6*, 181–211.
35. Lee, C.-Y.; McCammon, J. A.; Rossky, P. J. The structure of liquid water at an extended hydrophobic surface. *J. Chem. Phys.* **1984**, *80*, 4448–4455.
36. Chen, J.; Schusteritsch, G.; Pickard, C. J.; Salzmann, C. G.; Michaelides, A. Two Dimensional Ice from First Principles: Structures and Phase Transitions. *Phys. Rev. Lett.* **2016**, *116*, 025501.
37. Jaffe, R. L.; Gonnet, P.; Werder, T.; Walther, J. H.; Koumoutsakos, P. Water–Carbon Interactions 2: Calibration of Potentials using Contact Angle Data for Different Interaction Models. *Mol. Sim.* **2004**, *30*, 205–216.

38. Pérez-Hernández, G.; Schmidt, B. Anisotropy of the water–carbon interaction: molecular simulations of water in low-diameter carbon nanotubes. *Phys. Chem. Chem. Phys.* **2013**, *15*, 4995–5006.
39. Kaukonen, M.; Gulans, A.; Havu, P.; Kauppinen, E. Lennard-Jones parameters for small diameter carbon nanotubes and water for molecular mechanics simulations from van der Waals density functional calculations. *J. Comp. Chem.* **2012**, *33*, 652–658.
40. Hummer, G.; Rasaiah, J. C.; Noworyta, J. P. Water conduction through the hydrophobic channel of a carbon nanotube. *Nature* **2001**, *414*, 188–190.
41. Werder, T.; Walther, J. H.; Jaffe, R. L.; Halicioglu, T.; Koumoutsakos, P. On the Water-Carbon Interaction for Use in Molecular Dynamics Simulations of Graphite and Carbon Nanotubes. *J. Phys. Chem. B* **2003**, *107*, 1345–1352.
42. Wang, P.; Gao, W.; Cao, Z.; Liechti, K. M.; Huang, R. Numerical Analysis of Circular Graphene Bubbles. *J. Appl. Mech.* **2013**, *80*, 040905–040905.
43. Springman, R. M.; Bassani, J. L. Snap transitions in adhesion. *J. Mech. Phys. Solids* **2008**, *56*, 2358–2380.
44. Mostaani, E.; Drummond, N. D.; Fal’ko, V. I. Quantum Monte Carlo Calculation of the Binding Energy of Bilayer Graphene. *Phys. Rev. Lett.* **2015**, *115*, arXiv: 1506.08920.
45. Vasu, K. S.; Prestat, E.; Abraham, J.; Dix, J.; Kashtiban, R. J.; Beheshtian, J.; Sloan, J.; Carbone, P.; Neek-Amal, M.; Haigh, S. J. et al. Van der Waals pressure and its effect on trapped interlayer molecules. *Nature Comm.* **2016**, *7*, 12168.
46. Otani, M.; Sugino, O. First-principles calculations of charged surfaces and interfaces: A plane-wave nonrepeated slab approach. *Phys. Rev. B* **2006**, *73*, 115407.
47. Giannozzi, P.; Baroni, S.; Bonini, N.; Calandra, M.; Car, R.; Cavazzoni, C.; Davide Ceresoli,; Chiarotti, G. L.; Cococcioni, M.; Dabo, I. et al. QUANTUM ESPRESSO: a modular and open-

- source software project for quantum simulations of materials. *J. Phys.: Condens. Matter* **2009**, *21*, 395502.
48. Gillan, M. J.; Alfè, D.; Michaelides, A. Perspective: How good is DFT for water? *J. Chem. Phys.* **2016**, *144*, 130901.
49. Dion, M.; Rydberg, H.; Schröder, E.; Langreth, D. C.; Lundqvist, B. I. Van der Waals Density Functional for General Geometries. *Phys. Rev. Lett.* **2004**, *92*, 246401.
50. Thonhauser, T.; Cooper, V. R.; Li, S.; Puzder, A.; Hyldgaard, P.; Langreth, D. C. Van der Waals density functional: Self-consistent potential and the nature of the van der Waals bond. *Phys. Rev. B* **2007**, *76*, 125112.
51. Román-Pérez, G.; Soler, J. M. Efficient Implementation of a van der Waals Density Functional: Application to Double-Wall Carbon Nanotubes. *Phys. Rev. Lett.* **2009**, *103*, 096102.
52. Sabatini, R.; Küçükbenli, E.; Kolb, B.; Thonhauser, T.; Gironcoli, S. d. Structural evolution of amino acid crystals under stress from a non-empirical density functional. *J. Phys.: Condens. Matter* **2012**, *24*, 424209.
53. Klimeš, J.; Bowler, D. R.; Michaelides, A. Van der Waals density functionals applied to solids. *Phys. Rev. B* **2011**, *83*, 195131.
54. Radha, B.; Esfandiar, A.; Wang, F. C.; Rooney, A. P.; Gopinadhan, K.; Keerthi, A.; Mishchenko, A.; Janardanan, A.; Blake, P.; Fumagalli, L. et al. Molecular transport through capillaries made with atomic scale precision. *arXiv:1606.09051 [cond-mat]* **2016**, arXiv: 1606.09051.

Graphical TOC Entry

